

UC Irvine

UC Irvine Previously Published Works

Title

Pyrazole-Based Acid Ceramidase Inhibitors: Design, Synthesis, and Structure–Activity Relationships

Permalink

<https://escholarship.org/uc/item/7hc7x3wf>

Journal

Synthesis, 48(17)

ISSN

0039-7881

Authors

Diamanti, Eleonora
Bottegoni, Giovanni
Goldoni, Luca
[et al.](#)

Publication Date

2016

DOI

10.1055/s-0035-1561456

Copyright Information

This work is made available under the terms of a Creative Commons Attribution License, available at <https://creativecommons.org/licenses/by/4.0/>

Peer reviewed

Pyrazole-Based Acid Ceramidase Inhibitors: Design, Synthesis, and Structure–Activity Relationships

Eleonora Diamanti^a
 Giovanni Bottegoni^a
 Luca Goldoni^a
 Natalia Realini^a
 Chiara Pagliuca^a
 Fabio Bertozzi^a
 Daniele Piomelli^{*a,b}
 Daniela Pizzirani^a



^a Drug Discovery and Development, Fondazione Istituto Italiano di Tecnologia, via Morego 30, 16163 Genova, Italy

^b Departments of Anatomy and Neurobiology, Pharmacology and Biological Chemistry, University of California, Irvine, CA 92697, USA
 daniele.piomelli@iit.it

Dedicated to Professor Stuart L. Schreiber on the occasion of his 60th birthday

Received: 24.02.2016

Accepted after revision: 18.04.2016

Published online: 09.06.2016

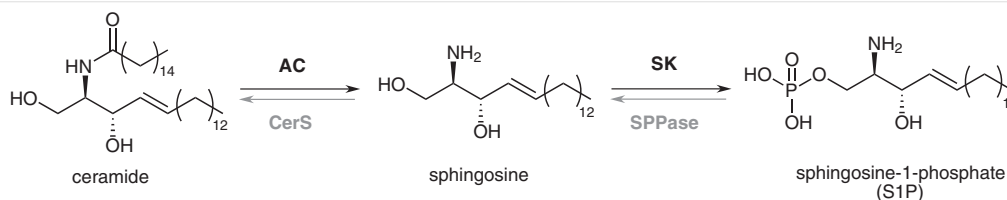
DOI: 10.1055/s-0035-1561456; Art ID: ss-2016-z0135-fa

Abstract Acid ceramidase (AC) is a lysosomal cysteine amidase responsible for the cleavage of ceramide into sphingosine, which is then phosphorylated to sphingosine 1-phosphate. AC regulates the intracellular levels of ceramide and sphingosine, and AC inhibition may be useful in the treatment of disorders, such as cancer, in which ceramide-mediated signaling may be dysfunctional. Despite their potential experimental and therapeutic value, the number of available small-molecule inhibitors of AC activity remains limited. In the present study is described the discovery of a class of potent pyrazole carboxamide-based AC inhibitors, which were identified using the atomic property field (APF) approach and developed through systematic SAR investigations and in vitro pharmacological characterization. The best compound of this series inhibits AC with nanomolar potency and causes ceramide accumulation and sphingosine depletion in intact G361 proliferative melanoma cells. By expanding the current armamentarium of AC inhibitors, these results should facilitate future efforts to unravel the biology of AC and the therapeutic potential of its inhibition.

Key words acid ceramidase, ceramides, atomic property field (APF), regioisomers, structure–activity relationship (SAR), melanoma

The sphingolipids are ubiquitous lipid constituents of eukaryotic cell membranes.¹ In addition to this essential structural function, sphingolipids are also thought to play multiple signaling roles and to be involved in the pathogenesis of cancer,² inflammation,³ and neuropathic pain.⁴ In particular, two key sphingolipids – ceramides and sphingosine 1-phosphate (S1P) – have been shown to regulate cell fate in opposite manner: ceramides by mediating cellular senescence⁵ and apoptosis,⁶ and S1P by promoting cell survival and proliferation.⁷

The ceramides are a highly heterogeneous family of *N*-acylated sphingosines with long-chain fatty acids.⁸ They hold a central role in sphingolipid metabolism and are the metabolic precursors of S1P; conversion of one into the other has been proposed to serve as a ‘rheostat’ in the regulation of cell fate.⁹ The lysosomal lipid amidase, acid ceramidase (AC, encoded by the *ASAH-1* gene) is a key element of this rheostat. It catalyzes the hydrolysis of ceramides into fatty acid and sphingosine, which is then converted into S1P by sphingosine kinase (SK) (Scheme 1).¹⁰



Scheme 1 A simplified overview of the sphingolipid rheostat. Representative ceramide species (d18:1/16:0). AC: acid ceramidase; CerS: ceramide synthase; SK: sphingosine kinase; SPPase: sphingosine phosphate phosphatase.

Biographical Sketches



(Authors shown clockwise from top left) **Daniela Pizzirani** is Scientist in the Medicinal Chemistry Lead Optimization Team at Chiesi Farmaceutici. After receiving her undergraduate degree in Pharmaceutical Chemistry and Technology, she performed her graduate studies in medicinal chemistry at the University of Bologna. Following completion of her doctoral studies, she joined the group of Professor Stuart L. Schreiber at Harvard University as a postdoctoral associate in 2007. In 2010, she moved to the Italian Institute of Technology (IIT), working as Medicinal Chemist in the group of Professor Daniele Piomelli.

Daniele Piomelli is the holder of Louise Turner Arnold Chair in Neurosciences and Professor of Anatomy and Neurobiology, Pharmacology and Biological Chemistry at the University of California, Irvine. In addition, he is the founding director of the unit of drug discovery and development (D3) at the Italian Institute of Technology in Genoa, Italy.

Eleonora Diamanti received her Master's degree in medicinal chemistry at the University of Camerino in 2010. She joined in 2012 Professor Piomelli's group at the Italian Institute of Technology (IIT, Genova, Italy) for her Ph.D. During her doctoral course she spent 10 months at the University of Bristol under the supervision of Professor V. K. Aggarwal. She is currently a post doc at the IIT.

Dr. Chiara Pagliuca earned her Ph.D. in

organic chemistry from Florence University, where she worked on the synthesis and development of new molecules for targeted tumor diagnosis and therapy. She has most recently completed a series of post-doc assignments leading drug development projects for international research institutions, including the Italian Institute of Technology. Her scientific investigation has ranged from hit identification, hit-to-lead, and lead optimization programs to the preclinical development of new molecular entities. She has co-authored 16 publications and holds 4 patent applications. Dr. Pagliuca is currently working as a Scientist at a global player of the chemical industry.

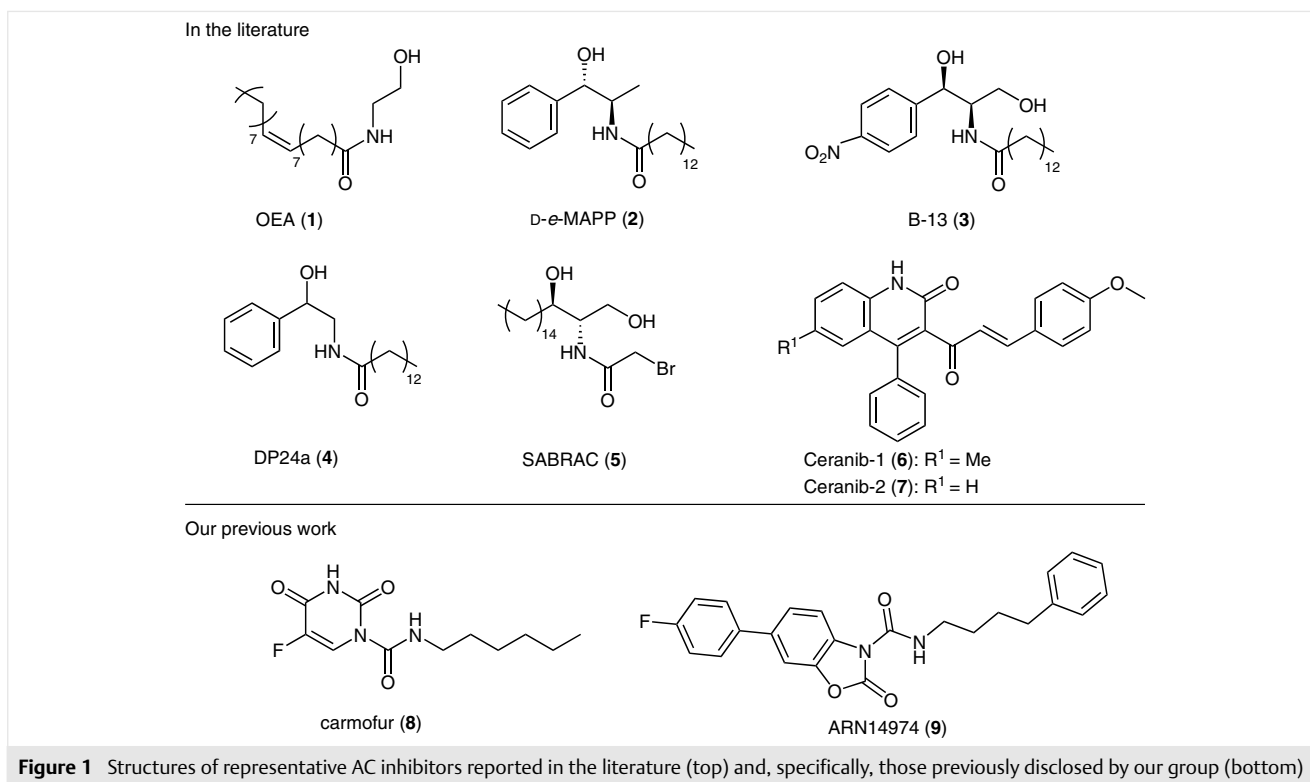
Fabio Bertozzi received his Ph.D. in organic chemistry from the University of Pisa, Italy in 2002. He then joined ACADIA Pharmaceuticals (Denmark) for a post-doctoral fellowship aiming at the development of novel methodologies for the synthesis of drug-like structures. After more than five years at Acadia Pharmaceuticals as medicinal chemist working on several projects at the hit confirmation/lead optimization stage in the field of CNS related diseases, Dr. Bertozzi joined the Istituto Italiano di Tecnologia (Genova, Italy) in late 2009 to coordinate the medicinal chemistry efforts on different drug discovery projects.

Giovanni Bottegoni received his Ph.D. in pharmaceutical sciences from the University of Bologna, Italy in 2006. For two years, he was post-doc at The Scripps Research Insti-

tute in La Jolla, California (USA), and then he joined the Istituto Italiano di Tecnologia (Genova, Italy) first as a post-doc and later as a team leader. He is the author of over 40 publications and co-inventor in several patents. In 2015, he was awarded the DCF prize for medicinal chemistry by the medicinal chemistry division of the Italian chemical society.

Dr. Luca Goldoni received his Ph.D. in drug discovery from the University of Genova (Italy) in 2016, focused on metabolomics by NMR spectroscopy, under the guidance of Professor Piomelli. He gained 12 years of experience as an NMR technician in several chemical and pharmaceutical companies. In 2011 he joined the Italian Institute of Technology (IIT) as NMR senior specialist where he is currently responsible for the structure elucidation of new chemical entities, and their purity evaluation. From 2013 his research interest also included metabolomics by NMR spectroscopy.

Dr. Natalia Realini got her Master's degree in biology applied to medical science and her Ph.D. in medical pharmacology, toxicology and chemotherapy. In 2010, she joined Professor Piomelli's group at the University of California, Irvine and she's currently a senior postdoctoral associate at the Italian Institute of Technology, Genova, Italy. Her research interests include sphingolipid biology, mainly focused on the biological role of acid ceramidase in health and diseases.



Since inhibition of AC increases the cellular levels of ceramides and concomitantly decreases those of sphingosine and S1P, it represents a potential strategy to address disorders associated with abnormal levels of these bioactive lipids – including certain types of cancer and inflammation.

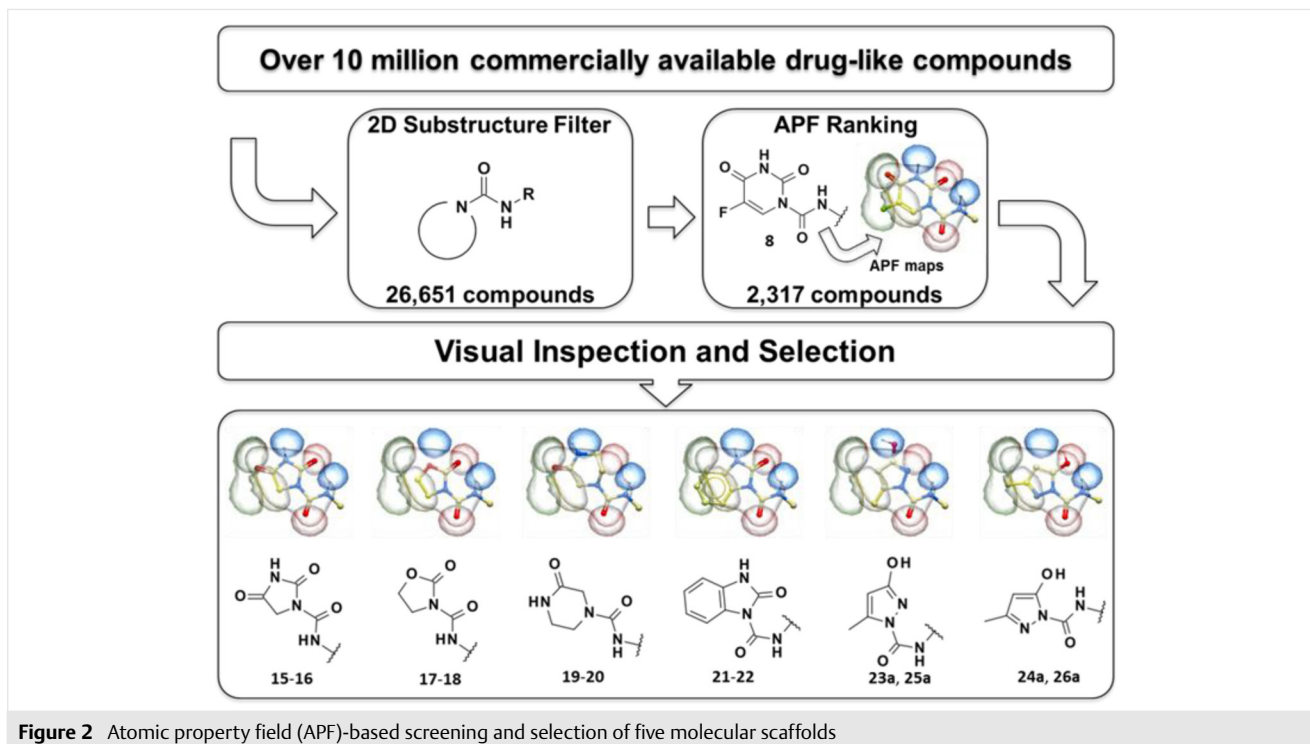
A relatively small number of AC inhibitors have been reported in the scientific and patent literature.¹¹ Ceramide analogues such as oleoylethanolamide (OEA, **1**, $K_i \approx 500 \mu\text{M}$),¹² D-erythro-2-(*N*-myristoylamino)-1-phenyl-1-propanol (D-*e*-MAPP, **2**, $\text{IC}_{50} > 500 \mu\text{M}$), and B-13 (**3**, $\text{IC}_{50} = 10 \mu\text{M}$),¹³ are not drug-like and display low inhibitory potencies (Figure 1).

Structural modifications of these molecules have led to the discovery of significantly more potent compounds, such as DP24a (**4**)¹⁴ ($\text{IC}_{50} = 1.3 \mu\text{M}$ on human recombinant AC) and SABRAC (**5**),¹⁵ which inhibit AC activity in intact cells and cell lysates with nanomolar potency.

Among the AC inhibitors that are not structurally related to ceramide, Ceranib-1 and 2 (**6,7**)¹⁶ show micromolar potency towards intracellular ceramidases, inhibit cell proliferation and induce cell death in certain types of cancer, alone or in combination with paclitaxel. In addition, cystatin SA (encoded in humans by the *CST2* gene) is a physiological inhibitor of AC ($K_i \approx 5 \mu\text{M}$), which binds the enzymes and creates an allosteric interference with the active site domains.¹⁷

Previous work in our laboratory has identified two new classes of potent small-molecule inhibitors of AC (Figure 1). The first includes substituted 2,4-dioxypyrimidine-*N*1-carboxamides such as carmofur (**8**), which inhibits AC activity with nanomolar potency.¹⁸

Members of this class act synergistically with standard anti-neoplastic drugs to stop proliferation of various types of cancer cells, suggesting a potential clinical use as chemosensitizers.¹⁸ Recently, we have shown that *N*3-carbamoyl uracil derivatives may be useful in normalizing ceramide levels and concomitantly sensitize proliferative melanoma cells to the cytotoxic actions of various anti-tumoral agents. These results are suggestive of the potential utility of AC blockade as chemosensitizing strategy in proliferative melanoma.¹⁹ Another class of AC inhibitors identified by our laboratory includes benzoxazolone-carboxamide derivatives, which display improved chemical and metabolic stability, compared to carmofur and its congeners.²⁰ Focused structure-activity relationship (SAR) studies around the benzoxazolone-carboxamide scaffold have led to the identification of 6-(4-fluorophenyl)-2-oxo-*N*-(4-phenylbutyl)-1,3-benzoxazole-3-carboxamide (ARN14974, **9**, $\text{IC}_{50} = 0.079 \mu\text{M}$) as a highly potent systemically active inhibitor of intracellular AC activity.²⁰ Expanded SAR investigations confirmed the potential for benzoxazolone-carboxamide derivatives to provide stable and systemically active inhibitors of AC.²¹



Despite these advances, the number of molecular scaffolds that have demonstrated utility as AC inhibitors remains very limited. Yet, broadening chemical diversity in this class of molecules is essential not only to expand our ability to study the roles of ceramide and S1P in living animals, but also to support possible preclinical and clinical development efforts.

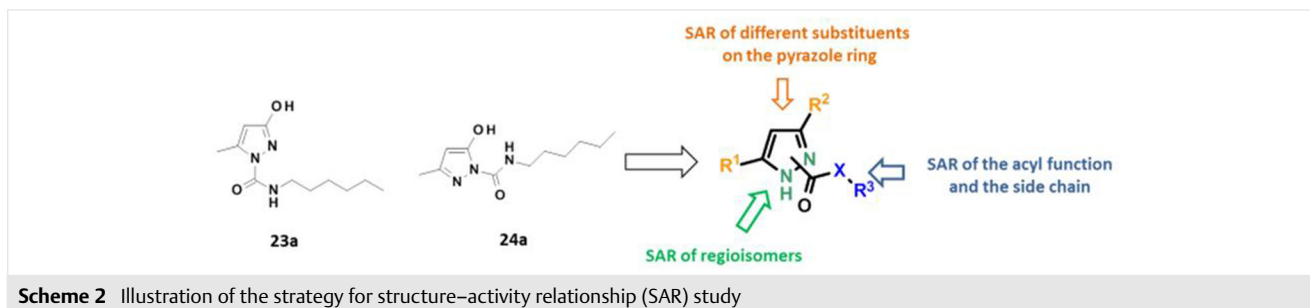
To identify novel molecular scaffolds for AC inhibition, in the present study, we utilized the atomic property field (APF) method²² using carmofur (**8**) as a template. Five distinct heterocyclic scaffolds **10–13** and **14a** were selected, which were functionalized as *N*-carboxamides to yield a small set of 12 compounds: **15–22**, **23a–24a**, **25a–26a** (Figure 2).

The ability of these molecules to inhibit AC activity was examined using lysates of HEK293 cells that overexpressed human AC (h-AC). We obtained promising results with the

pyrazole derivatives **23a–26a** (Table 2, *vide infra*), and selected this chemical class for further expansion. Our initial structure–activity relationship (SAR) studies were focused on compounds **23a** and **24a** (Scheme 2), investigating the effects of various substituents at positions 3 and 5 of the pyrazole ring as well as the role of the acyl function and side chain length. When two isomeric pyrazole *N*-carboxamides were obtained, the regiochemistry-based SARs were also evaluated. Finally, the potent inhibitor **24n** was selected for *in vitro* pharmacology studies and its ability was tested to interfere with AC activity in intact G361 cells, a human melanoma cell line characterized by a proliferative phenotype.

Chemistry

In analogy to hit compounds **8** and **9**, we coupled the selected heterocyclic scaffolds **10–13** and **14a** with hexyl and phenylbutyl isocyanate to obtain the corresponding *N*-car-



boxamide derivatives **15–22** and **23a–26a**, in good yields (Scheme S1, Supporting Information and Table 2). The acylation of asymmetrically substituted pyrazolol **14a** takes place competitively at both nitrogen atoms of the pyrazole ring giving a mixture of two regioisomers **23a–24a** and **25a–26a**, in overall good yield and in a ratio of 8:92 and 7:93, respectively. The regioisomers were separated by column chromatography, and the structures assigned by spectroscopic analysis. No traces of *O*-acylated products were found.

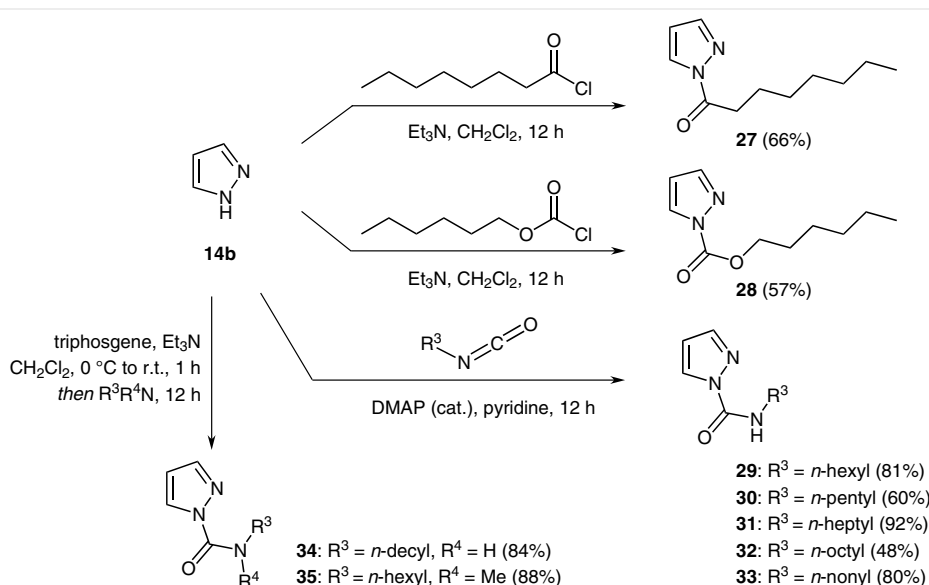
Focusing on the pyrazole scaffold, the three *N*-acyl derivatives **27–29** were first synthesized by coupling commercial unsubstituted pyrazole **14b** to octanoyl chloride, hexyl chloroformate, and hexyl isocyanate, respectively (Scheme 3).

Next, the syntheses of a series of unsubstituted and differently substituted pyrazole *N*-carboxamide derivatives are outlined in Scheme 3 and Table 1. A small set of compounds **30–35**, bearing *N*-carboxamide alkyl chains of different length, was prepared as shown in Scheme 3. The unsubstituted pyrazole **14b** was coupled to various alkyl isocyanates in pyridine at room temperature, in the presence of a catalytic amount of DMAP, to give derivatives **30–33**. For compounds **34** and **35**, **14b** was first activated with triphosgene followed by in situ quenching with *n*-decylamine and *N*-methylhexylamine, respectively (Scheme 3). Then, we focused on the synthesis of mono- and disubstituted pyrazole *N*-carboxamides. Table 1 shows the reaction conditions adopted for the coupling of a series of substituted pyrazoles **14c–t** with hexyl isocyanate to afford compounds **23c–o**, the corresponding regioisomers **24c–f**, **24h**, **24k–o**, and derivatives **36–40** as single isomers, in moderate to good yields.

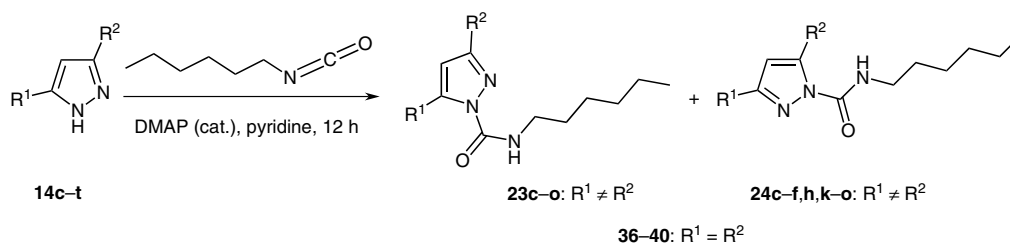
For the asymmetrically substituted pyrazoles **14c–o**, a mixture of two regioisomers **23** and **24** was obtained in all cases, with the exception of 3-phenyl-, 3-trifluoromethyl- and 3-nitro-1*H*-pyrazoles **14g,i,j**, which reacted forming only one isomer **23g,i,j** (Table 1). The ratio between the two *N*-acyl compounds **23** and **24** is found to be affected by a combination of electronic and steric factors of the substituents in position 3 and 5 of the pyrazole ring.²³ Indeed, in the presence of an electron-donating group, such as methyl, both pyrazole nitrogen atoms undergo acylation giving a mixture of the two possible regioisomers, in which the predominant one is the less sterically hindered compound, namely **23d** and **24d** (Table 1). In contrast, the effect of an electron-withdrawing group, such as trifluoromethyl, decreases the reactivity of the neighboring nitrogen atom leading to the formation of only one regioisomer, which also corresponds to the less bulky derivative, namely **23i** (Table 1). In the cases of pyrazoles having substituents comparable in size but with different electronic properties, such as methyl and trifluoromethyl groups, both nitrogen atoms participate in the acylation reaction, which also occurs at the nitrogen atom neighboring the electron-withdrawing moiety, as for **23n** and **24n** (Table 1).

Unambiguous assignment of the regiochemistry of asymmetrically substituted pyrazole *N*-carboxamides was achieved by NMR analysis. A set of 1D (¹H NMR, ¹³C NMR) and 2D experiments (¹H–¹H COSY, ¹H–¹³C HSQC, ¹H–¹³C HMBC and ¹H–¹⁵N HMBC) on purified regioisomers provided robust evidence for structural elucidation (Figure 3).

We observed that acylation of one nitrogen atom of the pyrazole system implies (i) a marked ¹H-downfield shift of the adjacent substituent due to anisotropic effect exerted by the carbonyl group of the urea moiety,²⁴ (ii) a ¹⁵N-high-



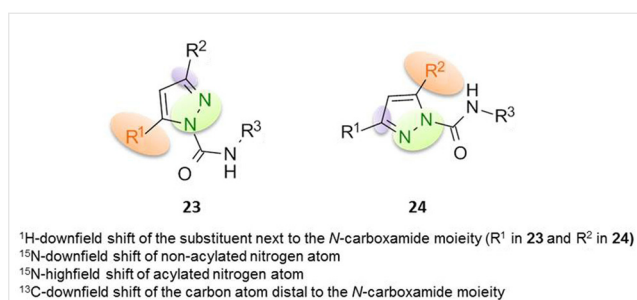
Scheme 3 Synthesis of unsubstituted pyrazole *N*-acyl derivatives **27–35**

Table 1 Synthesis of Mono- and Disubstituted Pyrazole-*N*-carboxamides **23c–o**, **24c–f**, **24h**, **24k–o**, **36–40**

Entry	14	R ¹	R ²	Products (yield) ^a	Ratio (23/24) ^b
1	14c	H	OH	23c (25%) 24c (14%)	67:33
2	14d	H	Me	23d (65%) 24d (14%)	66:34
3	14e	H	NH ₂	23e (11%) 24e (50%)	14:86
4	14f	H	OMe	23f (75%) 24f (2%)	92:8
5	14g	H	Ph	23g (54%) –	–
6	14h	H	Br	23h (54%) 24h ^c	92:8
7	14i	H	CF ₃	23i (82%) –	–
8	14j	H	NO ₂	23j (62%) –	–
9	14k	Me	NH ₂	23k (4%) 24k (89%)	6:94
10	14l	Me	OMe	23l (6%) 24l (2%)	70:30
11	14m	Me	Br	23m (55%) 24m (8%)	70:30
12	14n	Me	CF ₃	23n (66%) 24n (6%)	92:8
13	14o	Me	Ph	23o (75%) 24o ^c	93:7
14	14p	Me	Me	36 (74%)	
15	14q	Et	Et	37 (81%)	
16	14r	<i>n</i> -Pr	<i>n</i> -Pr	38 (83%)	
17	14s	<i>i</i> -Pr	<i>i</i> -Pr	39 (71%)	
18	14t	<i>t</i> -Bu	<i>t</i> -Bu	40 (quant)	

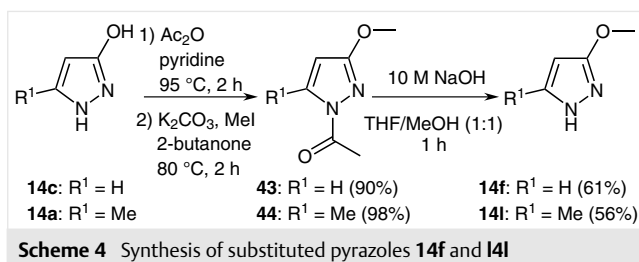
^a Yields refer to purified products.^b Ratio between regioisomers was determined by ¹H NMR of the crude mixture.^c Not isolated.

field shift of the acylated nitrogen atom (≈ 220 ppm), while the non-acylated nitrogen resonates at lower field (≈ 290 ppm),²⁵ and (iii) a ¹³C-downfield shift of the carbon atom distal to the urea moiety (Figure 3). Cross-correlation of

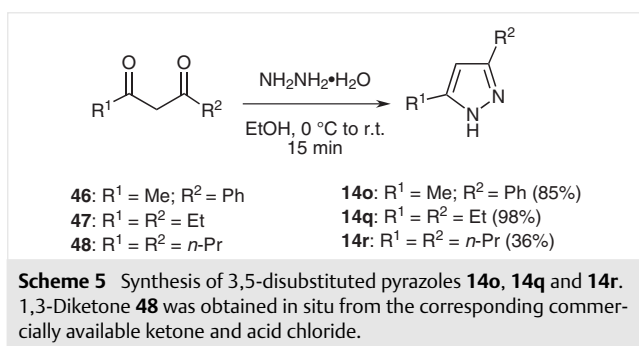
**Figure 3** Spectroscopic evidence for structure assignment of regioisomers **23** and **24**

these evidences, consistently found throughout regioisomer series **23** and **24**, allowed building a robust spectroscopic method for structural elucidation of these compounds. In those cases when one regioisomer is formed, structural assignment was based on the comparison between spectroscopic data collected for the single isomer and the corresponding non-acylated pyrazole (see the Supporting Information for complete structural assignment of representative substituted pyrazole-*N*-carboxamides).

Pyrazoles that were not commercially available were prepared as shown in Schemes 4 and 5. 3-Methoxy-1*H*-pyrazole (**14f**) and 3-methoxy-5-methyl-1*H*-pyrazole (**14l**) were synthesized through a three-step sequence starting from the corresponding hydroxyl pyrazoles **14c** and **14a**, respectively (Scheme 4).



These compounds were first reacted with 1 equivalent of acetic anhydride to afford *N*1-acetyl pyrazoles **41** and **42** as single isomers. Methylation with iodomethane under basic conditions proceeded smoothly to give compounds **43** and **44**, which upon cleavage of the acetyl group delivered the desired methoxypyrazoles **14f** and **14l** in overall good yield. Finally, a Knorr-type reaction was adopted to synthesize pyrazoles **14o**, **14q**, and **14r**.²⁶ Cyclocondensation of the proper 1,3-dicarbonyl compounds **46–48** with hydrazine led to the desired pyrazoles in good to excellent yields (Scheme 5).



Results and Discussion

The primary objective of the present study was to discover novel chemical classes of small-molecule inhibitors of lysosomal AC activity. We utilized the computer-assisted APF method – starting from carmofur (**8**) as a template – to identify novel scaffolds that, while structurally different, match the pharmacophore fingerprint of **8**. From ZINC,²⁷ we retrieved a library of over 10 million rule-of-five compliant compounds (Figure 2).²⁸ To guarantee synthetic accessibility, the selected dataset encompassed only commercially available derivatives. First, the library was pre-filtered by means of a simple two-dimensional query, retrieving only those molecules bearing a ureidic group matching the one displayed by **8**. A total of 26,651 compounds were selected, and assigned a pseudoenergy score that expressed their fit into the APF fields generated using **8** as template (see Computational Methods). This score expressed the best possible overlap of the following six properties: hydrogen bond donor propensity, hydrogen bond acceptor propensity, sp² carbon atom hybridization, lipophilicity, size, and electro-negativity. Since **8** is a neutral molecule, the charge field

usually included in APF calculations was not taken into consideration. To select the compounds to prioritize, we arbitrarily set a threshold for the pseudoenergy value at –1200 score units. This value, which is two-thirds of the 1800 score units assigned to compound **8** into its own APF field, represented a good compromise between prioritizing a limited number of compounds and extending the selection beyond those derivatives just trivially resembling **8** without introducing any element of true novelty. Eventually 2317 compounds proceeded to medicinal-chemistry-guided visual inspection. Five distinct molecular scaffolds were selected based on (i) structural diversity, (ii) ease of preparation, and (iii) efficient access to structural analogues for SAR purposes (Figure 2). Scaffolds **10–13** and **14a**, displaying monocyclic and bicyclic as well as heteroaliphatic and heteroaromatic systems, were functionalized as *N*-carboxamide derivatives **15–22**, **23a–26a** and screened against h-AC in a fluorescence-based assay²⁹ (Table 2).

Compounds **15–20** having a heterocyclic scaffold such as hydantoin, oxazolidinone, and piperazinone did not significantly inhibit AC at 10 μM. Similarly, no inhibition was seen for compounds **21** and **22**, obtained from the heteroaromatic bicycle dihydrobenzimidazolone. By contrast, *N*-carboxamides of 3-hydroxy-5-methylpyrazole **23a** and **24a** and **25a** and **26a** showed a marked degree of inhibitory activity. These compounds showed median inhibitory concentration (IC₅₀) values in the low micromolar range, and an interesting difference in activity between regioisomers (e.g., **23a**, IC₅₀ = 3.137 μM vs **24a**, IC₅₀ = 0.455 μM, Table 5, *vide infra*).³⁰ Based on these results, we selected **23a** and **24a** as starting points for our SAR analysis.

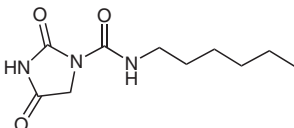
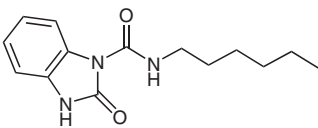
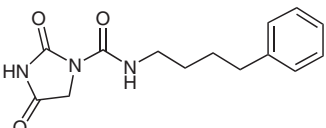
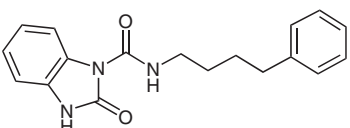
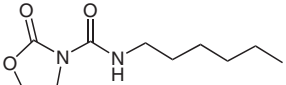
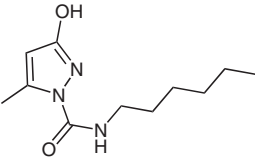
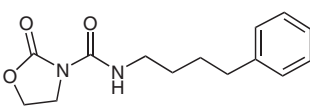
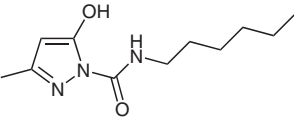
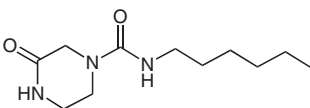
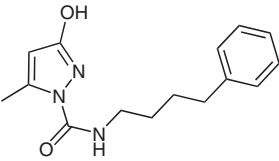
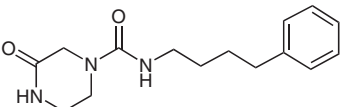
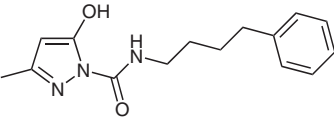
The pyrazole-*N*-carboxamides were tested for their ability to inhibit the hydrolysis of *N*-[(1*S*,2*R*)-2-hydroxy-1-(hydroxymethyl)-4-(2-oxochromen-7-yl)oxybutyl]dodecanamide by recombinant h-AC in a fluorescence-based assay. IC₅₀ values are reported in Tables 3–5.

We first investigated the role of acyl function and side chain. This study was conducted on the unsubstituted pyrazole ring to better appreciate possible changes in potency while avoiding influences due to substituents on the heterocycle and regioisomer formation. The unsubstituted pyrazole-*N*-carboxamide **29**, bearing a six-carbon alkyl chain, was found to be moderately potent (IC₅₀ = 0.481 μM, Table 3).

The corresponding amide **27** and carbamate **28** derivatives showed no inhibitory activity. Similarly inactive was the *N*-Me derivative **35**, where the 1-carboxamide NH moiety of **29** was substituted with a methyl group (Table 3).

Having assessed that the 1-carboxamide NH is mandatory for activity, we investigated the influence of side-chain length by preparing a small set of derivatives **30–34** with different number of carbon atoms in the side chain. A decrease in chain length, as in *N*-pentylpyrazole-1-carboxamide (**30**) (IC₅₀ = 1.39 μM), was associated with a decrease in inhibitory potency. Conversely, increasing the length of the chain from six to nine methylene units led to progressively

Table 2 Screening of Compounds 15–22, 23a–26a on Human AC

Compd	Structure	% Inh at 10 μ M	Compd	Structure	% Inh at 10 μ M
15		61	21		no inhibition
16		11	22		no inhibition
17		6	23a		96
18		11	24a		98
19		37	25a		94
20		16	26a		92

higher potency, with the *N*-nonyl derivative **33** showing the best IC_{50} value (0.197 μ M) within this set of compounds. Further extension of the chain length to ten methylene units had an opposite effect (**34**, IC_{50} = 0.993 μ M).

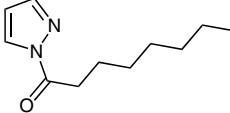
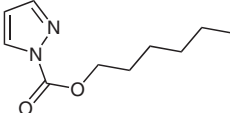
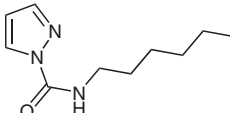
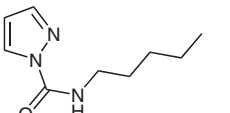
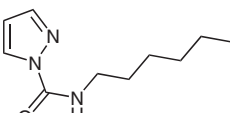
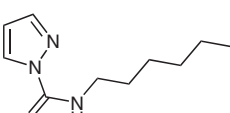
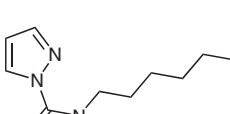
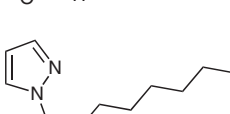
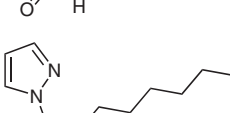
Next, we focused on substitutions of the pyrazole ring. Considering that the initial hit compounds, **23a** and **24a**, bear a hydroxyl and a methyl group at positions 3 and 5, respectively, we started our analysis by removing one group at the time to obtain the monosubstituted 3- and 5-hydroxy **23c** and **24c** and 3- and 5-methyl derivatives **23d** and **24d** (Table 4).

The 3-substituted compounds **23c** and **23d** showed an inhibitory potency in the micromolar range; the corresponding regioisomers **24c** and **24d** turned out to be 6- to 12-fold more potent than **23c** and **23d**, displaying IC_{50} values of 0.196 μ M and 0.169 μ M, respectively, and 2-fold more potent than hit compound **24a** (IC_{50} = 0.455 μ M). To further explore the effect of an electron-donating group on the pyrazole ring, the amino and methoxy-substituted de-

rivatives **23e** and **24e**, and **23f** and **24f** were synthesized. Interestingly, we did not observe significant difference in potency between regioisomers **23e** and **24e**, which inhibited AC with an IC_{50} of 0.216 μ M and 0.522 μ M, respectively. Although regioisomer **23e** was more potent than **24e**, the difference in IC_{50} was only two-fold. Conversely, methylation of the hydroxyl group caused a substantial drop in potency, as the 3-methoxy derivative **23f** only partially inhibited AC at 10 μ M; its isomer **24f** showed a limited chemical stability and was not tested. Replacement of the hydroxyl group with a bulkier, but planar moiety, such as a phenyl, led to the single isomer **23g**, which inhibited AC with moderate potency (IC_{50} = 0.766 μ M).

Continuing our study on the effect of monosubstitution of the pyrazole, we turned to electron-withdrawing groups, as shown with compounds **23h–23i**, obtained as single isomers (Table 4). The presence of bromine at position 3 led to a compound which was equipotent to **23c** (**23h**, IC_{50} = 2.49

Table 3 Inhibitory Potencies (IC_{50}) of Compounds **27–35** on Human AC^a

Compd	Structure	IC_{50} (μM) \pm S.E.M
27		no inhibition
28		no inhibition
29		0.481 ± 0.029
30		1.390 ± 0.280
31		0.224 ± 0.054
32		0.208 ± 0.049
33		0.197 ± 0.032
34		0.993 ± 0.264
35		no inhibition

^a IC_{50} values are reported as mean values of two or more determinations.

μM), while a trifluoromethyl group turned out to be well tolerated, as derivative **23i** showed an IC_{50} value of 0.110 μM , being the most potent compound of this set.

As a continuation of the SAR study, we investigated the effect of disubstitution at position 3 and 5 of the pyrazole ring (Table 5). As methyl-substituted derivatives **23d** and

24d were found to be slightly more potent than the pyrazole carboxamides **23c** and **24c**, and with the objective of removing an additional chemical handle suitable for acylation, we maintained the methyl substituent and replaced the hydroxyl group with those electron-donating and electron-withdrawing moieties studied in the monosubstituted series of compounds. We observed that disubstitution of the pyrazole ring generally enhances inhibitory potency against AC and is associated to significant differences in activity between the two isomeric series of compounds. The combination of methyl group with both electron-donating and electron-withdrawing moieties was generally well tolerated, delivering compounds with submicromolar potencies, with the exception of derivative **23i**, which showed a 4-fold drop in potency with respect to hit **23a**, confirming the detrimental effect of a methoxy group on this scaffold for AC inhibition. Of particular interest were the results obtained with the 3-methyl-5-bromo- and 3-methyl-5-trifluoromethyl-substituted derivatives **24m** and **24n**, which showed IC_{50} values of 0.011 μM and 0.014 μM , respectively, representing the most potent compounds within this series (Table 5).

Finally, the activity of a small set of symmetric 3,5-disubstituted pyrazole derivatives **36–40** bearing progressively bulkier alkyl substituents was investigated (Table 6).

All the compounds showed double-digit nanomolar potency toward AC indicating that steric hindrance is generally well tolerated, with the exception of the less potent 3,5-dipropyl derivative **38** ($IC_{50} = 0.294 \mu\text{M}$). The highest activity within this small series was observed with compound **40** bearing a *tert*-butyl group at positions 3 and 5 ($IC_{50} = 0.011 \mu\text{M}$).

At the outset, we set as goal of our project the diversification of the available arsenal of small-molecule inhibitors of AC that can be used as tools to investigate the biology of this enzyme and, possibly, as starting points for therapeutic candidates. Having elucidated the main SAR features of this new chemical class, our efforts were focused on its pharmacological characterization. The highly potent inhibitor **24n** was selected for this purpose and its stability was assessed in buffer and mouse plasma (Table 7).

Compound **24n** displayed adequate chemical stability both at acidic and neutral pH, as well as in cell culture media. Conversely, the compound had very limited stability in mouse plasma (half-life, $t_{1/2} = 9$ min), making it a promising candidate for 'soft drug' applications (e.g., topical skin or lung delivery).

Accordingly, the compound was tested in the proliferative melanoma cell line G361. We selected this line based on previous work, which had shown that AC regulation of ceramide signaling is important in melanoma cell viability.¹⁹ The cells were incubated in the presence of **24n** (0.1–20 μM) and AC inhibition and sphingolipid levels were measured after various incubation times (Figure 4).

Table 4 Inhibitory Potencies (IC_{50}) of Compounds **23c–i** and **24c–f** on Human AC^a

Compd	Structure	IC_{50} (μM) \pm S.E.M	Compd	Structure	IC_{50} (μM) \pm S.E.M
23c		2.461 \pm 1.256	24c		0.196 \pm 0.099
23d		1.100 \pm 0.270	24d		0.169 \pm 0.046
23e		0.216 \pm 0.010	24e		0.522 \pm 0.087
23f		32% at 10 μM	24f		unstable
23g		0.766 \pm 0.326			
23h		2.492 \pm 2.108			
23i		0.110 \pm 0.025			

^a IC_{50} values are reported as mean values of two or more determinations.

The compound caused a rapid concentration-dependent inhibition of AC activity in these cells. Notably, **24n** inhibited cellular AC activity at concentration as low as 0.1 μM , and the inhibition was already appreciable after 15 minutes of incubation and persisted for 6 hours, with a partial recovery of enzyme activity after 24 hours (Figure 4, A and B).

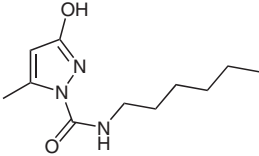
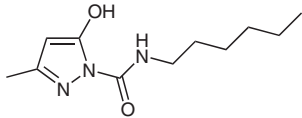
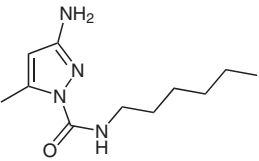
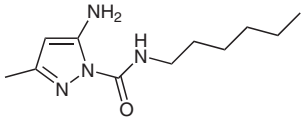
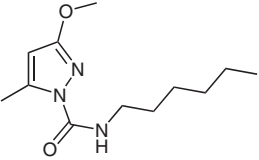
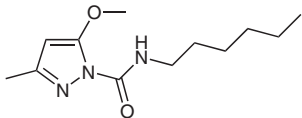
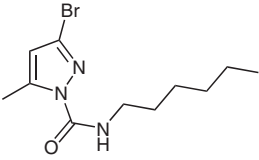
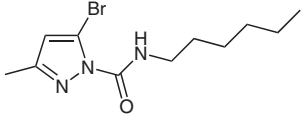
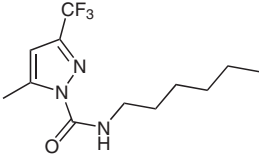
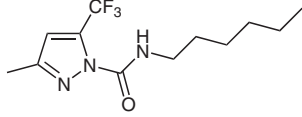
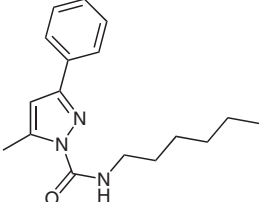
This level of efficacy compares well with those reported for other classes of AC inhibitors.¹⁹ As expected, AC inhibition was accompanied by accumulation of various species of ceramides: specifically, we observed a significant increase of those (dihydro)ceramides, which are preferred substrates for AC (namely, d18:0/16:0 and d18:1/16:0) and a concen-

tration-dependent decrease in sphingosine (Figure 4, C). At the highest concentration of **24n** tested (20 μM), we observed a time-dependent accumulation of ceramide, which reached a maximum after 6 hours, and a rapid decrease in sphingosine levels, which was already detectable after 15 minutes (Figure 4, D). Increases in sphingomyelins and glucosylceramide were also observed after 15 min (Figure S4 in the Supporting Information). The results demonstrate that **24n** is able to effectively inhibit AC in a complex cellular environment.

Conclusions

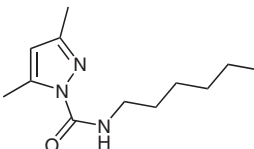
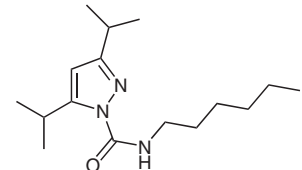
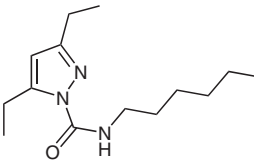
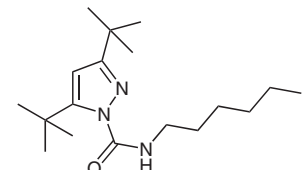
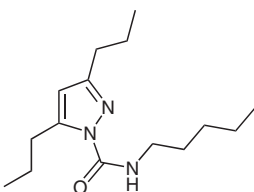
In the present study, we utilized the APF-based computer-assisted approach to identify novel scaffolds that may serve as starting points for the design of small-molecule inhibitors of AC activity. Using carmofur (**8**) as a template, we probed the ZINC library and retrieved compounds that, while structurally different, match the pharmacophore fingerprint of **8**. Medicinal chemistry-guided visual inspection of a set of computationally selected compounds identified five distinct scaffolds that, when appropriately functionalized, revealed substituted pyrazole carboxamides as promising novel AC inhibitors. A series of differently substituted

Table 5 Inhibitory Potencies (IC_{50}) of Compounds **23a**, **23k–o**, **24a**, **24k–n**, and **36–40** on Human AC^a

Compd	Structure	IC_{50} (μM) \pm S.E.M	Compd	Structure	IC_{50} (μM) \pm S.E.M
23a		3.137 ± 0.585	24a		0.455 ± 0.112
23k		0.489 ± 0.173	24k		0.218 ± 0.065
23l		14.11 ± 0.30	24l		unstable
23m		0.264 ± 0.072	24m		0.010 ± 0.001
23n		0.108 ± 0.020	24n		0.014 ± 0.010
23o		0.317 ± 0.065			

^a IC_{50} values are reported as mean values of two or more determinations.

Table 6 Inhibitory Potencies (IC_{50}) of Compounds **36–40** on Human AC^a

Compd	Structure	IC_{50} (μM) \pm S.E.M	Compd	Structure	IC_{50} (μM) \pm S.E.M
36		0.074 \pm 0.037	39		0.043 \pm 0.003
37		0.062 \pm 0.006	40		0.011 \pm 0.001
38		0.294 \pm 0.046			

^a IC_{50} values are reported as mean values of two or more determinations.

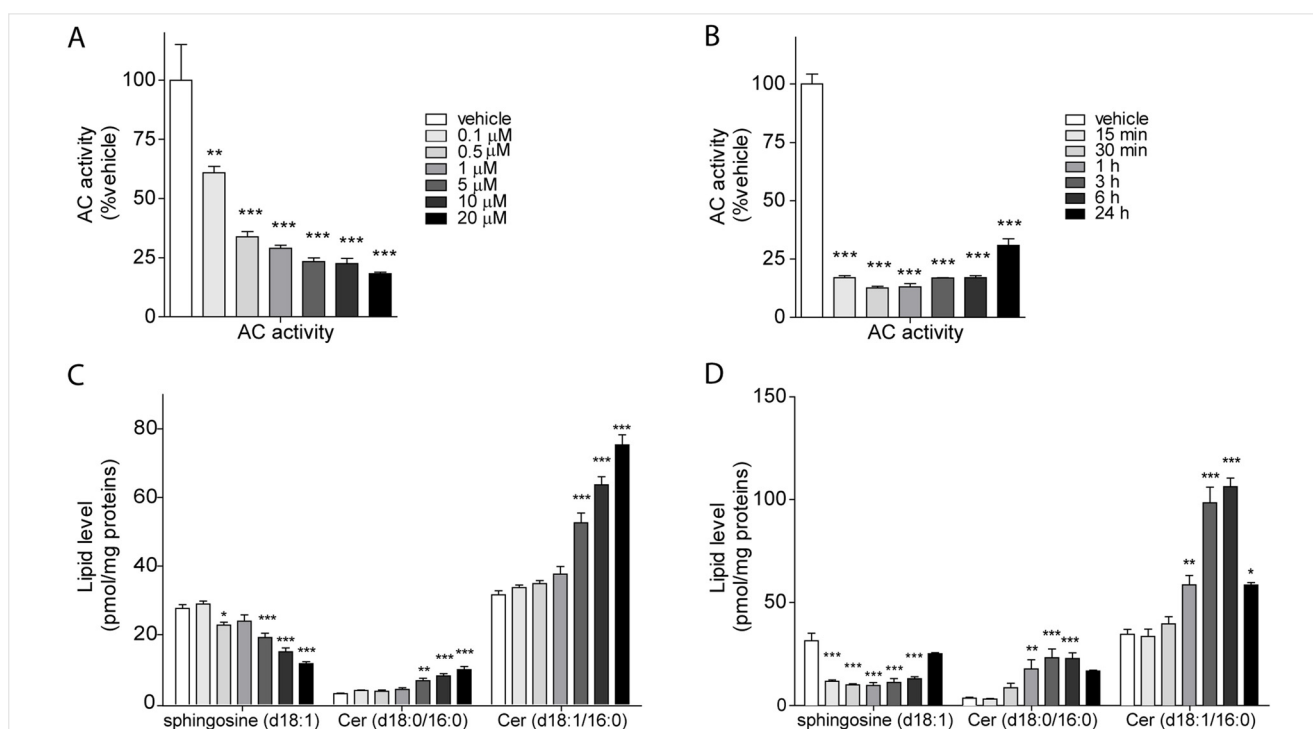


Figure 4 Effects of compound **24n** in proliferative melanoma cells G361. Concentration dependence of the effect on AC activity (A) and sphingolipid levels (C). Time-course of the effect of **24n** (20 μM) on AC activity (B) and sphingolipid levels (D). Values are reported as the mean \pm S.E.M of 3–6 determinations. Independent experiments yielded similar results. * $p < 0.05$, ** $p < 0.01$, *** $p < 0.001$ vs vehicle; one-way ANOVA followed by Dunnett's test.

Table 7 Stability of Compound **24n** by LC-MS Analysis

Compound	Buffer stability (pH 4.5) ^a $t_{1/2}$ (min)	Buffer stability (pH 7.4) ^b $t_{1/2}$ (min)	Cell media stability ^c $t_{1/2}$ (min)	m-Plasma stability ^d $t_{1/2}$ (min)
24n	>360	66	>360	9

^a NaCl (150 mM), NaH₂PO₄ (100 mM), trisodium citrate (100 mM), NP40 (1%), DTT (3 mM).

^b PBS (phosphate buffered saline).

^c DMEM (Dulbecco's Modified Eagle's Medium)

^d Mouse plasma, 37 °C.

derivatives were synthesized and an NMR-based model was built to unambiguously assign the regiochemistry of *N*-acylation on the pyrazole ring. A systematic SAR study around the new scaffold highlighted structural features that are important for AC inhibition. We observed that an unsubstituted nitrogen atom in the carboxamide moiety is mandatory for activity, and assessed the best length for the alkylic side chain as nine methylene units. The electronic nature of substituents on the pyrazole ring does not significantly impact the inhibitory potency toward AC, as both electron-donating and electron-withdrawing moieties are tolerated, with the exception of the methoxy group that leads to inactive or unstable compounds **23f–24f**, **23i–24i**. Conversely, the regiochemistry of acylation turned out to be critical, as a 2- to 10-fold difference in potency was generally observed between the two series of regioisomers **23** and **24**. Finally, one of the most potent compounds identified, **24n**, was selected for further characterization. Stability analysis of this derivative suggested its potential use for 'soft drug' applications and, thus, it was tested on proliferative melanoma cells G361. The compound **24n** effectively engages AC in these cells leading to the expected variations in the sphingolipid profile. This novel chemical class further expands and complements the available armamentarium of chemical tools to study the biology of AC and may offer promising candidates for the development of topical treatments for cancers and other hyperproliferative disorders of the skin.

All the commercially available reagents and solvents were used as purchased from vendors without further purification. Anhydrous solvents (pyridine, CH₂Cl₂, DMSO) were purchased from Sigma-Aldrich. Automated column chromatography purifications were done using a Teledyne ISCO apparatus (CombiFlash® Rf) with prepacked silica gel columns of different sizes (from 4 g up to 40 g). Mixtures of increasing polarity of cyclohexane and EtOAc were used as eluents. Purifications by preparative HPLC-MS were run on a Waters Autopurification system consisting of a 3100 Single Quadrupole Mass Spectrometer equipped with an Electrospray Ionization interface and a 2998 Photodiode Array Detector. HPLC system included a 2747 Sample Manager, 2545 Binary Gradient Module, System Fluidic Organizer and 515 HPLC Pump. PDA range was 210–400 nm. Purifications were performed on a XBridge™ Prep C₁₈ OBD column (100 × 19 mmID, particle size 5 μm) with a XBridge™ Prep C₁₈ (10 × 19 mmID, particle size 5 μm) guard cartridge. Mobile phase was 10 mM NH₄OAc in MeCN/H₂O (95:5) at pH 5. Electrospray ionization in positive and negative mode

was used. NMR experiments were run on a Bruker Avance III 400 system (400.13 MHz for ¹H, and 100.62 MHz for ¹³C), equipped with a BBI probe and Z-gradients. Spectra were acquired at 300 K, using DMSO-*d*₆ or CDCl₃ as solvents. UPLC-MS analyses were run on a Waters ACQUITY UPLC-MS system consisting of an SQD (single quadrupole detector) mass spectrometer equipped with an Electrospray Ionization interface and a Photodiode Array Detector. PDA range was 210–400 nm. Analyses were performed on an ACQUITY UPLC HSS T3 C₁₈ column (50 × 2.1 mmID, particle size 1.8 μm) with a VanGuard HSS T3 C₁₈ precolumn (5 × 2.1 mmID, particle size 1.8 μm). Mobile phase was either 10 mM NH₄OAc in H₂O at pH 5 adjusted with AcOH (A) and 10 mM NH₄OAc in MeCN/H₂O (95:5) at pH 5 (B). Electrospray ionization in positive and negative mode was applied. All final compounds, **15–22**, **23a**, **23c–23o**, **24a**, **24c–24f**, **24h**, **24i–24p**, **25a**, **26a**, and **27–40** showed ≥95% purity by NMR and UPLC-MS analysis.

Pyrazole-*N*-carboxamides 23a, 23c–23e, 23h, 23i, 23k, 23m–23n, 24a, 24c–24e, 24h, 24k, 24m, 24n, 29, 33, 36, 37, and 40; General Procedure (Tables 1 and 3–5, Scheme 3)

The properly substituted pyrazole (1.0 equiv) was dissolved in anhyd pyridine. DMAP (0.1 equiv) was added, and the reaction mixture was stirred under N₂ for 30 min. The appropriate isocyanate (1.1–1.5 equiv) was then added, and the resulting mixture was stirred for 12 h. The solvent was evaporated under reduced pressure and the crude was purified by silica gel column chromatography, eluting with a mixture cyclohexane/EtOAc.

***N*-Hexyl-3-hydroxy-5-methylpyrazole-1-carboxamide (23a) and *N*-Hexyl-5-hydroxy-3-methylpyrazole-1-carboxamide (24a)**

The reaction was carried out following the general procedure previously described, dissolving **14a** (0.30 g, 3.06 mmol) in anhyd pyridine (10 mL) and employing hexyl isocyanate (0.49 mL, 3.36 mmol). The two regioisomers **23a–24a** were obtained in a ratio of 8:92, determined by ¹H NMR of the crude. The mixture was separated by silica gel column chromatography to afford **23a** (cyclohexane/EtOAc, 80:20) and **24a** (cyclohexane/EtOAc, 50:50). **23a** (0.02 g, 4%) as a white powder; mp 59.5 °C.

¹H NMR (400 MHz, CDCl₃): δ = 0.89 (t, *J* = 6.7 Hz, 3 H), 1.23–1.43 (m, 6 H), 1.53–1.65 (m, 2 H), 2.55 (s, 3 H), 3.33 (q, *J* = 6.8 Hz, 2 H), 5.62 (s, 1 H), 4.96 (br s, 1 H), 6.54 (t, *J* = 5.7 Hz, 1 H).

¹³C NMR (101 MHz, CDCl₃): δ = 14.1, 14.7, 22.7, 26.6, 29.7, 31.6, 40.5, 97.2, 146.2, 151.1, 161.4.

MS (ESI): *m/z* = 226 [M + H]⁺, 248 [M + Na]⁺.

MS (ESI): *m/z* = 224 [M – H][–].

24a

Yield: 0.51 g (75%); white powder; mp 108 °C.

^1H NMR (101 MHz, CDCl_3): δ = 11.39 (s, 1 H), 8.85–9.42 (m, 1 H), 5.15 (s, 1 H), 3.22–3.39 (m, 2 H), 2.21 (s, 3 H), 1.48–1.66 (m, 2 H), 1.18–1.38 (m, 6 H), 0.75–0.90 (m, 3 H).

^{13}C NMR (101 MHz, CDCl_3): δ = 164.2, 150.0, 149.9, 92.6, 39.9, 31.4, 29.6, 26.6, 12.2, 22.5, 14.0.

MS (ESI): m/z = 226 [M + H] $^+$, 248 [M + Na] $^+$.

MS (ESI): m/z = 224 [M – H] $^-$.

***N*-Hexyl-3-hydroxypyrazole-1-carboxamide (23c) and *N*-Hexyl-5-hydroxypyrazole-1-carboxamide (24c)**

The reaction was carried out following the general procedure described above, dissolving **14c** (0.30 g, 3.56 mmol) in anhyd pyridine (17.8 mL) and employing hexyl isocyanate (0.57 mL, 3.92 mmol). The two regioisomers **23c** and **24c** were obtained in a ratio of 67:33, determined by ^1H NMR of the crude. The mixture was separated by HPLC-MS.

23c

Yield: 0.19 g (25%); light yellow powder; mp 88 °C.

^1H NMR (400 MHz, CDCl_3): δ = 8.04 (d, J = 2.9 Hz, 1 H), 6.45 (t, J = 5.4 Hz, 1 H), 5.88 (d, J = 2.9 Hz, 1 H), 3.38 (td, J = 5.9, 7.1 Hz, 2 H), 1.52–1.70 (m, 2 H), 1.21–1.48 (m, 6 H), 0.89 (t, J = 6.7 Hz, 3 H).

^{13}C NMR (101 MHz, CDCl_3): δ = 163.1, 149.7, 131.4, 96.5, 40.7, 31.6, 29.6, 26.5, 22.7, 14.1.

MS (ESI): m/z = 212 [M + H] $^+$, 234 [M + Na] $^+$, 250 [M + K] $^+$.

MS (ESI): m/z = 210 [M – H] $^-$.

24c

Yield: 0.11 g (14%); white powder; mp 85 °C.

^1H NMR (101 MHz, CDCl_3): δ (major rotamer) = 0.89 (t, J = 6.7 Hz, 3 H), 1.27–1.44 (m, 6 H), 1.53–1.69 (m, 2 H), 3.38 (q, J = 7.0 Hz, 2 H), 5.50 (app s, 1 H), 7.34 (app s, 1 H), 9.03 (m, 1 H), 10.38 (s, 1 H); δ (minor rotamer) = 0.89 (t, J = 6.7 Hz, 3 H), 1.27–1.44 (m, 6 H), 1.53–1.69 (m, 2 H), 3.38 (q, J = 7.0 Hz, 2 H), 5.44 (app s, 1 H), 7.06 (m, 1 H), 7.48 (app s, 1 H); 1:0.7 ratio of two rotamers.

^{13}C NMR (101 MHz, CDCl_3): two rotamers: δ (major rotamer) = 156.79, 149.86, 142.30, 88.09, 39.97, 31.53, 29.61, 26.58, 22.66, 14.13; δ (minor rotamer) = 163.86, 149.88, 137.49, 94.76, 40.10, 31.53, 29.61, 26.58, 22.66, 14.13.

MS (ESI): m/z = 212 [M + H] $^+$, 234 [M + Na] $^+$, 250 [M + K] $^+$.

MS (ESI): m/z = 210 [M – H] $^-$.

***N*-Hexyl-3-methylpyrazole-1-carboxamide (23d) and *N*-Hexyl-5-methylpyrazole-1-carboxamide (24d)**

The reaction was carried out following the general procedure described above, dissolving **14d** (0.05 mL, 0.61 mmol) in anhyd pyridine (6.1 mL) and employing hexyl isocyanate (0.13 mL, 0.91 mmol). The two regioisomers **23d** and **24d** were obtained in a ratio of 66:34, determined by ^1H NMR of the crude. The mixture was separated by silica gel column chromatography to afford **23d** (cyclohexane/EtOAc, 92:8) and **24d** (cyclohexane/EtOAc, 95:5).

23d

Yield: 0.08 g (65%); colorless oil.

^1H NMR (400 MHz, CDCl_3): δ = 8.09 (d, J = 2.6 Hz, 1 H), 7.07 (m, 1 H), 6.16 (d, J = 2.6 Hz, 1 H), 3.38 (td, J = 6.0, 7.2 Hz, 2 H), 2.28 (s, 3 H), 1.51–1.69 (m, 2 H), 1.24–1.43 (m, 6 H), 0.88 (t, J = 6.0 Hz, 3 H).

^{13}C NMR (101 MHz, CDCl_3): δ = 152.0, 150.0, 129.3, 108.6, 40.4, 31.6, 29.8, 26.6, 22.7, 14.1, 13.8.

MS (ESI): m/z = 210 [M + H] $^+$, 232 [M + Na] $^+$, 208 [M – H] $^-$.

24d

Yield: 0.02 g (14%); colorless oil.

^1H NMR (400 MHz, CDCl_3): δ = 7.41 (d, J = 1.5 Hz, 1 H), 7.32 (m, 1 H), 6.08 (m, 1 H), 3.36 (td, J = 6.0, 7.2 Hz, 2 H), 2.60 (s, 3 H), 1.53–1.70 (m, 2 H), 1.24–1.43 (m, 6 H), 0.87 (t, J = 7.0 Hz, 3 H).

^{13}C NMR (101 MHz, CDCl_3): δ = 151.4, 143.0, 140.4, 109.2, 40.3, 31.6, 29.7, 26.7, 22.7, 14.2, 14.1.

MS (ESI): m/z = 210 [M + H] $^+$, 228 [M + NH $_4$] $^+$.

MS (ESI): m/z = 208 [M – H] $^-$.

***3*-Amino-*N*-hexylpyrazole-1-carboxamide (23e) and *5*-Amino-*N*-hexylpyrazole-1-carboxamide (24e)**

The reaction was carried out following the general procedure described above, dissolving **14e** (0.20 g, 2.41 mmol) in anhyd pyridine (12 mL) and employing hexyl isocyanate (0.39 mL, 2.65 mmol). The two regioisomers **23e** and **24e** were obtained in a ratio of 14:86, determined by ^1H NMR of the crude. The mixture was separated by silica gel column chromatography to afford **23e** (cyclohexane/EtOAc, 60:40) and **24e** (cyclohexane/EtOAc, 70:30).

23e

Yield: 0.05 g (11%); yellow oil.

^1H NMR (400 MHz, CDCl_3): δ = 7.95 (d, J = 2.8 Hz, 1 H), 6.67–6.91 (m, 1 H), 5.77 (d, J = 2.7 Hz, 1 H), 3.45–3.67 (br s, 2 H), 3.34 (td, J = 5.9, 7.1 Hz, 2 H), 1.51–1.66 (m, 2 H), 1.25–1.39 (m, 6 H), 0.87 (t, J = 6.4 Hz, 3 H).

^{13}C NMR (101 MHz, CDCl_3): δ = 156.2, 150.1, 130.2, 98.1, 40.3, 31.6, 29.8, 26.6, 22.6, 14.1.

MS (ESI): m/z = 211 [M + H] $^+$, 233 [M + Na] $^+$.

24e

Yield: 0.25 g (50%); colorless oil.

^1H NMR (400 MHz, CDCl_3): δ = 7.26 (d, J = 1.1 Hz, 1 H), 7.07–7.23 (m, 1 H), 5.46–5.78 (br s, 2 H), 5.38 (d, J = 1.8 Hz, 1 H), 3.35 (td, J = 6.0, 7.1 Hz, 2 H), 1.52–1.68 (m, 2 H), 1.25–1.44 (m, 6 H), 0.89 (t, J = 6.6 Hz, 3 H).

^{13}C NMR (101 MHz, CDCl_3): δ = 153.0, 149.6, 141.2, 89.0, 40.0, 31.6, 29.7, 26.6, 22.7, 14.1.

MS (ESI): m/z = 211 [M + H] $^+$, 233 [M + Na] $^+$.

***3*-Bromo-*N*-hexylpyrazole-1-carboxamide (23h) and *5*-Bromo-*N*-hexylpyrazole-1-carboxamide (24h)**

The reaction was carried out following the general procedure described above, dissolving **14h** (0.15 g, 1.02 mmol) in anhyd pyridine (5.0 mL) and employing hexyl isocyanate (0.22 mL, 1.53 mmol). The two regioisomers **23h** and **24h** were obtained in a ratio of 92:8, determined by ^1H NMR of the crude. The mixture was separated by silica gel column chromatography to afford **23h** (cyclohexane/EtOAc, 99.5:0.5). Compound **24h** was not isolated.

23h

Yield: 0.10 g (54%); colorless oil.

^1H NMR (400 MHz, CDCl_3): δ = 0.88 (t, J = 6.9 Hz, 3 H), 1.23–1.42 (m, 6 H), 1.55–1.67 (m, 2 H), 3.39 (td, J = 6.0, 7.2 Hz, 2 H), 6.40 (d, J = 2.7 Hz, 1 H), 6.84–7.12 (m, 1 H), 8.11 (d, J = 2.7 Hz, 1 H).

^{13}C NMR (101 MHz, CDCl_3): δ = 148.7, 130.5, 129.8, 111.6, 40.7, 31.4, 29.6, 26.6, 22.6, 14.1.

MS (ESI): m/z = 272 and 274 [M – H]⁻.

N-Hexyl-3-(trifluoromethyl)pyrazole-1-carboxamide (23i)

The reaction was carried out following the general procedure described above, dissolving **14i** (0.15 g, 1.10 mmol) in anhyd pyridine (5.5 mL) and employing hexyl isocyanate (0.24 mL, 1.65 mmol). The crude was purified by silica gel column chromatography (cyclohexane/EtOAc, 90:10) to afford **23i** (0.24 g, 82%) as a colorless oil.

^1H NMR (400 MHz, CDCl_3): δ = 8.28 (d, J = 2.6 Hz, 1 H), 7.04–7.19 (m, 1 H), 6.64 (d, J = 2.7 Hz, 1 H), 3.43 (td, J = 6.0, 7.2 Hz, 2 H), 1.59–1.71 (m, 2 H), 1.25–1.36 (m, 6 H), 0.90 (t, J = 6.9 Hz, 3 H).

^{13}C NMR (101 MHz, CDCl_3): δ = 148.7, 144.9, 130.3, (q, J = 38.9 Hz), 120.6 (q, J = 269.7 Hz), 106.3 (q, J = 2.39 Hz), 50.8, 31.5, 29.6, 26.6, 22.6, 14.1.

MS (ESI): m/z = 264 [M + H]⁺, 286 [M + Na]⁺.

3-Amino-N-hexyl-5-methylpyrazole-1-carboxamide (23k) and 5-Amino-N-hexyl-3-methylpyrazole-1-carboxamide (24k)

The reaction was carried out following the general procedure described as above, dissolving **14k** (0.10 g, 1.03 mmol) in anhyd pyridine (5.1 mL) and employing hexyl isocyanate (0.165 mL, 1.13 mmol). The two regioisomers **23k** and **24k** were obtained in a ratio of 8:94, determined by ^1H NMR of the crude. The mixture was separated by silica gel column chromatography to afford **23k** (cyclohexane/EtOAc, 75:25) and **24k** (cyclohexane/EtOAc, 85:15).

23k

Yield: 0.009 g (4%); brown oil.

^1H NMR (400 MHz, CDCl_3): δ = 6.84–7.08 (m, 1 H), 5.53 (s, 1 H), 3.31 (q, J = 7.0 Hz, 2 H), 3.09–3.45 (br s, 2 H), 2.51 (s, 3 H), 1.46–1.74 (m, 2 H), 1.26–1.46 (m, 6 H), 0.88 (t, J = 6.7 Hz, 3 H).

^{13}C NMR (101 MHz, CDCl_3): δ = 154.2, 151.6, 144.7, 99.1, 40.1, 31.6, 29.9, 26.7, 22.7, 14.4, 14.2.

MS (ESI): m/z = 226 [M + H]⁺, 248 [M + Na]⁺, 264 [M + K]⁺.

MS (ESI): m/z = 224 [M – H]⁻.

24k

Yield: 0.21 g (89%); white powder; mp 63.5 °C.

^1H NMR (400 MHz, CDCl_3): δ = 7.05 (m, 1 H), 5.39 (br s, 2 H), 5.20 (s, 1 H), 3.13–3.45 (m, 2 H), 2.12 (s, 3 H), 1.49–1.72 (m, 2 H), 1.16–1.45 (m, 6 H), 0.88 (t, J = 7.0 Hz, 3 H).

^{13}C NMR (101 MHz, CDCl_3): δ = 153.1, 151.4, 150.0, 89.3, 39.9, 31.6, 29.8, 26.7, 22.7, 14.1.

MS (ESI): m/z = 225 [M + H]⁺, 247 [M + Na]⁺.

3-Bromo-N-hexyl-5-methylpyrazole-1-carboxamide (23m) and 5-Bromo-N-hexyl-3-methylpyrazole-1-carboxamide (24m)

The reaction was carried out following the general procedure described as above, dissolving **14m** (0.14 g, 0.85 mmol) in anhyd pyridine (2.6 mL) and employing hexyl isocyanate (0.18 mL, 1.27 mmol).

The two regioisomers **23m** and **24m** were obtained in a ratio of 70:30, determined by ^1H NMR of the crude. The mixture was separated by silica gel column chromatography to afford **23m** (cyclohexane/EtOAc, 99.5:0.5) and **24m** (cyclohexane/EtOAc, 90:10).

23m

Yield: 0.09 g (55%); colorless oil.

^1H NMR (400 MHz, CDCl_3): δ = 7.03–7.22 (m, 1 H), 6.13 (s, 1 H), 3.34 (td, J = 6.0, 7.2 Hz, 2 H), 2.59 (s, 3 H), 1.53–1.67 (m, 2 H), 1.23–1.44 (m, 6 H), 0.89 (t, J = 6.7 Hz, 3 H).

^{13}C NMR (101 MHz, CDCl_3): δ = 150.3, 145.2, 128.8, 112.2, 40.5, 31.6, 29.7, 26.7, 22.7, 14.2, 14.1.

MS (ESI): m/z = 288 and 290 [M + H]⁺.

24m

Yield: 0.012 g (8%); colorless oil.

^1H NMR (400 MHz, CDCl_3): δ = 7.26 (s, 1 H), 7.14–7.25 (m, 1 H), 3.35 (td, J = 6.0, 7.2 Hz, 2 H), 2.24 (s, 3 H), 1.55–1.68 (m, 2 H), 1.26–1.43 (m, 6 H), 0.89 (t, J = 6.5 Hz, 3 H).

^{13}C NMR (101 MHz, CDCl_3): δ = 151.7, 149.8, 113.8, 113.1, 40.5, 31.6, 29.7, 26.7, 22.7, 14.2, 14.0.

MS (ESI): m/z = 288 and 290 [M + H]⁺.

N-Hexyl-5-methyl-3-(trifluoromethyl)pyrazole-1-carboxamide (23n) and N-Hexyl-3-methyl-5-(trifluoromethyl)pyrazole-1-carboxamide (24n)

The reaction was carried out following the general procedure described as above, dissolving **14n** (0.30 g, 2.00 mmol) in anhyd pyridine (10 mL) and employing hexyl isocyanate (0.44 mL, 3.00 mmol). The two regioisomers **23n** and **24n** were obtained in a ratio of 92:8, determined by ^1H NMR of the crude. The mixture was separated by silica gel column chromatography to afford **23n** (cyclohexane/EtOAc, 96:4) and **24n** (cyclohexane/EtOAc, 94:6).

23n

Yield: 0.37 g (67%); colorless oil.

^1H NMR (400 MHz, CDCl_3): δ = 7.18–7.29 (m, 1 H), 6.35 (s, 1 H), 3.38 (td, J = 6.0, 7.3 Hz, 2 H), 2.64 (s, 3 H), 1.52–1.75 (m, 2 H), 1.23–1.48 (m, 6 H), 0.89 (t, J = 7.3 Hz, 3 H).

^{13}C NMR (101 MHz, CDCl_3): δ = 150.4, 144.9, 142.9, 120.8 (q, J = 269.6 Hz), 106.9, 40.6, 31.6, 29.6, 26.6, 22.7, 14.2, 14.1.

MS (ESI): m/z = 226 [M + H]⁺, 248 [M + Na]⁺, 264 [M + K]⁺.

MS (ESI): m/z = 224 [M – H]⁻.

24n

Yield: 0.03 g (6%); colorless oil.

^1H NMR (400 MHz, CDCl_3): δ = 7.15 (s, 1 H), 6.62 (s, 1 H), 3.42 (td, J = 6.1, 7.3 Hz, 2 H), 2.32 (s, 3 H), 1.55–1.72 (m, 2 H), 1.24–1.46 (m, 6 H), 0.91 (t, J = 6.30 Hz, 3 H).

^{13}C NMR (101 MHz, CDCl_3): δ = 149.5, 148.2, 133.8, 119.5 (q, J = 268.7 Hz), 112.3, 40.5, 31.4, 29.5, 26.5, 22.5, 14.0, 13.4.

MS (ESI): m/z = 225 [M + H]⁺, 247 [M + Na]⁺.

N-Hexylpyrazole-1-carboxamide (29)

The reaction was carried out following the general procedure described above, dissolving **14b** (0.12 g, 0.52 mmol) in anhyd pyridine (0.5 mL) and employing hexyl isocyanate (0.08 mL, 0.57 mmol). The crude was purified by silica gel column chromatography (cyclohexane/EtOAc, 90:10) to afford **29** (0.23 g, 81%) as a colorless oil.

¹H NMR (400 MHz, CDCl₃): δ = 8.22 (dd, *J* = 2.7, 0.8 Hz, 1 H), 7.59 (dd, *J* = 1.6, 0.8 Hz, 1 H), 7.15 (s, 1 H), 6.38 (dd, *J* = 2.7, 1.6 Hz, 1 H), 3.41 (td, *J* = 7.2, 6.0 Hz, 2 H), 1.58–1.69 (m, 2 H), 1.21–1.47 (m, 6 H), 0.82–1.00 (m, 3 H).

¹³C NMR (101 MHz, CDCl₃): δ = 149.8, 142.0, 128.7, 108.3, 40.5, 31.6, 29.8, 26.6, 22.7, 14.1.

MS (ESI): *m/z* = 194 [M – H]⁻.

N-Nonylpyrazole-1-carboxamide (33)

The reaction was carried out following the general procedure described above, dissolving **14b** (0.07 g, 1.03 mmol) in anhyd pyridine (1.0 mL) and employing nonyl isocyanate (0.30 mL, 1.54 mmol). The crude was purified by silica gel column chromatography (cyclohexane/EtOAc, 95:5) to afford **33** (0.19 g, 80%) as a white powder; mp 54 °C.

¹H NMR (400 MHz, CDCl₃): δ = 8.22 (d, *J* = 2.6 Hz, 1 H), 7.59 (d, *J* = 1.5 Hz, 1 H), 7.15 (s, 1 H), 6.38 (dd, *J* = 1.6, 2.7 Hz, 1 H), 3.41 (td, *J* = 6.0, 7.2 Hz, 2 H), 1.56–1.69 (m, 2 H), 1.19–1.44 (m, 12 H), 0.87 (t, *J* = 6.8 Hz, 3 H).

¹³C NMR (101 MHz, CDCl₃): δ = 150.2, 142.4, 129.0, 108.6, 40.8, 32.3, 30.1, 29.9, 29.7, 27.3, 23.1, 14.6.

MS (ESI) *m/z* = 238 [M + H]⁺.

MS (ESI): *m/z* = 236 [M – H]⁻.

N-Hexyl-3,5-dimethylpyrazole-1-carboxamide (36)

The reaction was carried out following the general procedure described as above, dissolving **14p** (0.10 g, 0.10 mmol) in anhyd pyridine (1.0 mL) and employing hexyl isocyanate (0.09 mL, 0.15 mmol). The crude was purified by silica gel column chromatography (cyclohexane/EtOAc, 99:1) to afford **36** (0.16 g, 74%) as a colorless oil.

¹H NMR (400 MHz, CDCl₃): δ = 7.19–7.25 (m, 1 H), 5.88 (s, 1 H), 3.34 (td, *J* = 6.0, 7.2 Hz, 2 H), 2.55 (s, 3 H), 2.19 (s, 3 H), 1.55–1.65 (m, 2 H), 1.27–1.42 (m, 6 H), 0.88 (t, *J* = 6.8 Hz, 3 H).

¹³C NMR (101 MHz, CDCl₃): δ = 151.5, 150.0, 143.6, 109.7, 40.2, 31.6, 29.8, 26.7, 22.7, 14.1, 13.7.

MS (ESI): *m/z* = 224 [M + H]⁺.

3,5-Diethyl-N-hexylpyrazole-1-carboxamide (37)

The reaction was carried out following the general procedure described as above, dissolving **14q** (0.10 g, 0.80 mmol) in anhyd pyridine (1.0 mL) and employing hexyl isocyanate (0.18 mL, 1.21 mmol). The crude was purified by silica gel column chromatography (cyclohexane/EtOAc, 90:10) to afford **37** (0.16 g, 81%) as a colorless oil.

¹H NMR (400 MHz, CDCl₃): δ = 7.20–7.26 (m, 1 H), 5.96 (s, 1 H), 3.34 (td, *J* = 6.0, 7.2 Hz, 2 H), 3.03 (q, *J* = 0.9, 7.4 Hz, 2 H), 2.57 (q, *J* = 7.6 Hz, 2 H), 1.53–1.67 (m, 2 H), 1.28–1.45 (m, 6 H), 1.24 (dt, *J* = 7.5, 9.2 Hz, 6 H), 0.88 (t, *J* = 6.9 Hz, 3 H).

¹³C NMR (101 MHz, CDCl₃): δ = 155.5, 151.4, 149.6, 105.7, 40.2, 31.9, 29.7, 26.5, 22.6, 21.6, 21.4, 14.3, 13.0.

MS (ESI): *m/z* = 252 [M + H]⁺.

3,5-Di-tert-butyl-N-hexyl-pyrazole-1-carboxamide (40)

The reaction was carried out following the general procedure described as above, dissolving **14t** (0.05 g, 0.27 mmol) in anhyd pyridine (2.7 mL) and employing hexyl isocyanate (0.06 mL, 0.40 mmol). The crude was purified by silica gel column chromatography (cyclohexane, 100%) to afford **40** (0.08 g, ~100%) as a colorless oil.

¹H NMR (400 MHz, CDCl₃): δ = 0.89 (t, *J* = 6.8 Hz, 3 H), 1.27 (s, 9 H), 1.30–1.42 (m, 6 H), 1.45 (s, 9 H), 1.55–1.68 (m, 2 H), 3.35 (td, *J* = 6.0, 7.3 Hz, 2 H), 6.02 (s, 1 H), 7.52 (s, 1 H).

¹³C NMR (101 MHz, CDCl₃): δ = 161.3, 156.4, 151.4, 104.7, 40.6, 33.1, 32.3, 31.6, 30.5, 30.1, 29.9, 29.6, 26.8, 22.7, 14.1.

MS (ESI): *m/z* = 308 [M + H]⁺, 228 [M + Na]⁺.

MS (ESI): *m/z* = 306 [M – H]⁻.

Computational Methods**APF Field Generation**

First, compound **8** was generated in three-dimensional structure within ICM (ICM3.7, Molsoft LLC, San Diego, CA, USA).³¹ Cartesian coordinates were translated into internal coordinates and MMFF³² force field atom types and charges were assigned. The starting conformation of compound **8** was obtained assigning an elongated orientation to the acyl side chain. Then, continuous three-dimensional pharmacophoric grid potentials were calculated accounting for relevant physico-chemical features of **8**. According to the original implementation reported by Totrov, seven APF potentials were selected: hydrogen bond donor and acceptor propensity, lipophilicity, size, charge, hybridization, and electronegativity. These grids encompassed the template molecule plus a 5 Å margin.

APF Screening

We retrieved a library of over ten million compounds from ZINC ('In-Stock', 'Drug-like' subset as of March 2011).²⁷ In ICM, this molecular dataset was prescreened by means of a 2D substructure query to retrieve all those compounds bearing a ureidic group having one nitrogen atom included in a ring system and the other as unsubstituted NH group. Selected compounds were automatically assigned three-dimensional internal coordinates, bond orders, tautomeric forms, stereochemistry, hydrogen atoms, protonation states, MMFF force field atom types, and charges by the ICM converting procedure. Then, the conformation of each compound was globally optimized using the biased probability Monte Carlo method within the precalculated APF field.³³ Torsional variables describing flexible rings were sampled explicitly. The intramolecular energy contribution was also considered to avoid unrealistically strained solutions. To provide a simulation of suitable length, the thoroughness parameter was set equal to the previously validated value of 1. Based on the fit of its optimized conformation into the APF field, each compound was assigned a pseudo-energy value and the library was ranked accordingly.

Pharmacology

Preparation of Enzyme-Enriched Lysate: Hek293 cells stably expressing human AC (Hek293-hAC)¹⁹ were suspended in 20 mM Tris-HCl (pH 7.5) with 0.32 M sucrose, sonicated and centrifuged at 800 g for 30 min at 4 °C. Supernatants were then centrifuged at 12 000 g for 30 min at 4 °C. Pellets were re-suspended in PBS buffer (pH 7.4) and subjected to three freeze-thaw cycles at –80 °C. The suspension was finally centrifuged at 105 000 g for 1 h at 4 °C and protein concentration was measured in the supernatant with bicinchoninic acid based protein assay.

Fluorescence-Based in Vitro Assay

Compounds were assessed for their ability to inhibit hydrolysis of the fluorogenic substrate, *N*-[(1*S*,2*R*)-2-hydroxy-1-(hydroxymethyl)-4-(2-oxochromen-7-yl)oxybutyl]dodecanamide, which is converted to umbelliferone by AC in the fluorescence-based in vitro assay, as previously described.^{20,34} Lysosomal lysate, enriched with AC, was prepared from Hek293 cells stably expressing human AC and preincubated with test compounds and a positive control (diluted 20 × from DMSO stock solutions at different concentrations) for 10 min. Then, the fluorogenic substrate (diluted 40 × from EtOH stock solution, final concentration 5 μM) was added and the mixture was incubated for 3 h at 37 °C, stopped with MeOH, and treated with NaIO₄ (fresh solution in 100 mM glycine/NaOH buffer pH 10.6) followed by 2 h incubation at 37 °C in the dark. Fluorescence intensities were measured (excitation/emission: 355/460 nm) and plotted as a function of compound concentrations. IC₅₀ values were calculated by nonlinear regression analysis using GraphPad Prism 5 (GraphPad Software Inc., CA, USA) applying a standard slope curve fitting. Fluorescence-based assay was used for in vitro IC₅₀ determinations.

AC Assay in Total Lysate

AC activity in G361 cells was performed using a previously described LC-MS based method.^{18a,20} Briefly, cells (10⁶ cells) were suspended in TENTN buffer (10 mM Tris-HCl pH 7.4, 150 mM NaCl, 1% Triton X100, 0.25% NP40, 2 mM EDTA, protease inhibitors), subjected to sonication and centrifuged at 800 g for 15 min at 4 °C. Supernatants were used as total lysates. Lysates (50–100 μg protein) were incubated in AC buffer (100 mM sodium phosphate, 0.1% Nonidet P-40, 150 mM NaCl, 3 mM DTT, 100 mM sodium citrate, pH 4.5) with 50 μM *N*-lauroyl ceramide (Nu-Chek Prep, Elysian, MN, USA) as substrate, reactions were carried on for 1 h at 37 °C. Reactions were stopped by addition of a mixture of CHCl₃/MeOH (2:1, v/v) containing 1 nmol 11-lauroleic acid (NuChek Prep). The organic phases were collected, dried under nitrogen and analyzed by UPLC/MS (Acquity, Waters) in the negative-ion mode monitoring the reaction product (lauric acid, *m/z* = 199) using 11-lauroleic acid as internal standard. Blank samples without protein extract or without substrate were used as negative controls.

Lipid Extraction

Lipids were extracted according to Bligh and Dyer.³⁵ Samples were transferred to glass vials and liquid-liquid extraction (LLE) was performed using a CHCl₃/MeOH mixture (1:2 v/v, 2 mL) with final 0.1% TFA, and spiked with internal standards (i.s.). After mixing for 30 s, CHCl₃ (0.6 mL) and H₂O (0.6 mL) were sequentially added and the samples were vortexed after each addition. The samples were centrifuged for 15 min at 3500 g at 4 °C. After centrifugation, the aqueous (upper) and organic (lower) phases were separated by a protein disk. The organic phase was transferred to glass vials. The aqueous fraction was extracted again with CHCl₃ (1 mL). Both organic phases were pooled, dried under N₂, and residues were redissolved in MeOH/CHCl₃ (9:1 v/v; 0.1 mL) and transferred to glass vials for analyses.

LC-MS Analyses

Samples were analyzed by LC-MS using an Acquity UPLC system coupled with Xevo TQ-MS triple-quadrupole mass spectrometer (Waters). Samples (3 μL) were loaded onto a waters acquity UPLC BEH column (2.1 × 50 mm, 1.7 μm) and metabolites were separated using a gradient elution at a flow rate of 0.4 mL/min. The mobile phase consisted of 0.1% formic acid in MeCN/H₂O (20:80, v/v) as solvent A and 0.1% formic acid in MeCN/*i*-PrOH (20:80, v/v) as solvent B. The MS system was operated in the ESI positive mode and analytes were

quantified in the multiple reaction monitoring (MRM) mode. The capillary voltage was set at 3 kV. The cone voltage was set at 25 V. The source temperature was set to 120 °C. Desolvation gas and cone gas (N₂) flow were set to 800 and 50 L/h, respectively. Desolvation temperature was set to 600 °C. Detection and analysis were controlled by Waters MassLynx software version 4.1. Calibration curves were prepared for every experiment. Data were normalized for protein concentration, measured using the bicinchoninic acid (BCA) assay (Pierce).

Cell Lines

G361 human melanoma cells were purchased from Sigma Aldrich, Milan, Italy. Cells were cultured at 37 °C and 5% CO₂ in Dulbecco's Modified Eagle's Medium (DMEM) containing 10% fetal bovine serum, 2 mM L-glutamine and antibiotics.

Sphingolipid Levels Measurement

Sphingolipids were quantified by LC-MS analysis according to the method previously described.³⁶

Acknowledgment

The authors thank Andrea Armirotti and Giuliana Ottonello for analytical stability data, Abdul Basit for sphingolipid level measurements, and Silvia Venzano for handling compounds.

Supporting Information

Supporting information for this article is available online at <http://dx.doi.org/10.1055/s-0035-1561456>.

References

- (1) (a) Hannun, Y. A.; Obeid, L. M. *Nat. Rev. Mol. Cell Biol.* **2008**, *9*, 139. (b) Bartke, N.; Hannun, Y. A. *J. Lipid Res.* **2009**, *50*, S91.
- (2) (a) Ogretmen, B.; Hannun, Y. A. *Nat. Rev. Cancer* **2004**, *4*, 604. (b) Gangoiti, P.; Camacho, L.; Arana, L.; Ouro, A.; Granada, M. H.; Brizuela, L.; Casas, J.; Fabrias, G.; Abad, J. L.; Delgado, A.; Gomez-Munoz, A. *Prog. Lipid Res.* **2010**, *49*, 316. (c) Ryland, L. K.; Fox, T. E.; Liu, X.; Loughran, T. P.; Kester, M. *Cancer Biol. Ther.* **2011**, *11*, 138. (d) Huang, W. C.; Chen, C. L.; Lin, Y. S.; Lin, C. F. *J. Lipids* **2011**, 565316. (e) Dimanche-Boitrel, M. T.; Rebillard, A. *Handb. Exp. Pharmacol.* **2013**, *216*, 73.
- (3) Maceyka, M.; Spiegel, S. *Nature* **2014**, *510*, 7503 58.
- (4) (a) Patti, G. J.; Yanes, O.; Shriver, L. P.; Courade, J. P.; Tautenhahn, R.; Manchester, M.; Siuzdak, G. *Nat. Chem. Biol.* **2012**, *8*, 232. (b) Salvemini, D.; Doyle, T.; Kress, M.; Nicol, G. *Trends Pharmacol. Sci.* **2013**, *34*, 110.
- (5) Huang, X.; Withers, B. R.; Dickson, R. C. *Biochim. Biophys. Acta* **2014**, *1841*, 657.
- (6) (a) Pettus, B. J.; Chalfant, C. E.; Hannun, Y. A. *Biochim. Biophys. Acta* **2002**, *1585*, 114. (b) Morales, A.; Lee, H.; Goni, F. M.; Kolesnick, R.; Fernandez-Checa, J. C. *Apoptosis* **2007**, *12*, 923.
- (7) (a) Zhang, H.; Desai, N. N.; Olivera, A.; Seki, T.; Brooker, G.; Spiegel, S. *J. Cell Biol.* **1991**, *114*, 155. (b) Payne, S. G.; Milstien, S.; Spiegel, S. *FEBS Lett.* **2002**, *531*, 54. (c) Spiegel, S.; Milstien, S. *Nat. Rev. Mol. Cell Biol.* **2003**, *4*, 397. (d) Takabe, K.; Spiegel, S. *J. Lipid Res.* **2014**, *55*, 1839.
- (8) Hannun, Y. A.; Obeid, L. M. *J. Biol. Chem.* **2011**, *286*, 27855.

- (9) (a) Cuvillier, O.; Pirianov, G.; Kleuser, B.; Vanek, P. G.; Coso, O. A.; Gutkind, S.; Spiegel, S. *Nature* **1996**, *381*, 6585 : 800. (b) Maceyka, M.; Payne, S. G.; Milstien, S.; Spiegel, S. *Biochim. Biophys. Acta* **2002**, *1585*, 193.
- (10) Gault, C. R.; Obeid, L. M.; Hannun, Y. A. *Adv. Exp. Med. Biol.* **2010**, *688*, 1.
- (11) (a) Saied, E. M.; Arenz, C. *Cell Physiol. Biochem.* **2014**, *34*, 197. (b) Nussbaumer, P. *ChemMedChem* **2008**, *3*, 543. (c) Saied, E. M.; Arenz, C. *Chem. Phys. Lipids* **2015**.
- (12) Bielawska, A.; Greenberg, M. S.; Perry, D.; Jayadev, S.; Shayman, J. A.; McKay, C.; Hannun, Y. A. *J. Biol. Chem.* **1996**, *271*, 12646.
- (13) Raisova, M.; Goltz, G.; Bektas, M.; Bielawska, A.; Riebeling, C.; Hossini, A. M.; Eberle, J.; Hannun, Y. A.; Orfanos, C. E.; Geilen, C. *FEBS Lett.* **2002**, *516*, 47.
- (14) Proksch, D.; Klein, J. J.; Arenz, C. *J. Lipids* **2011**, 971618.
- (15) Camacho, L.; Meca-Cortes, O.; Abad, J. L.; Garcia, S.; Rubio, N.; Diaz, A.; Celia-Terrassa, T.; Cingolani, F.; Bermudo, R.; Fernandez, P. L.; Blanco, J.; Delgado, A.; Casas, J.; Fabrias, G.; Thomson, T. M. *J. Lipid Res.* **2013**, *54*, 1207.
- (16) Draper, J. M.; Xia, Z.; Smith, R. A.; Zhuang, Y.; Wang, W.; Smith, C. D. *Mol. Cancer Ther.* **2011**, *10*, 2052.
- (17) Eliyahu, E.; Shtraizent, N.; He, X. X.; Chen, D. N.; Shalgi, R.; Schuchman, E. H. *J. Biol. Chem.* **2011**, *286*, 35624.
- (18) (a) Realini, N.; Solorzano, C.; Pagliuca, C.; Pizzirani, D.; Armirotti, A.; Luciani, R.; Costi, M. P.; Bandiera, T.; Piomelli, D. *Sci. Rep.* **2013**, *3*, 1035. (b) Pizzirani, D.; Pagliuca, C.; Realini, N.; Branduardi, D.; Bottegoni, G.; Mor, M.; Bertozzi, F.; Scarpelli, R.; Piomelli, D.; Bandiera, T. *J. Med. Chem.* **2013**, *56*, 3518.
- (19) Realini, N.; Palese, F.; Pizzirani, D.; Pontis, S.; Basit, A.; Bach, A.; Ganesan, A.; Piomelli, D. *J. Biol. Chem.* **2016**, *291*, 2422.
- (20) Pizzirani, D.; Bach, A.; Realini, N.; Armirotti, A.; Mengatto, L.; Bauer, I.; Giroto, S.; Pagliuca, C.; De Vivo, M.; Summa, M.; Ribeiro, A.; Piomelli, D. *Angew. Chem. Int. Ed.* **2015**, *54*, 485.
- (21) Bach, A.; Pizzirani, D.; Realini, N.; Vozella, V.; Russo, D.; Penna, I.; Melzig, L.; Scarpelli, R.; Piomelli, D. *J. Med. Chem.* **2015**, *58*, 9258.
- (22) Totrov, M. *Chem. Biol. Drug Des.* **2008**, *71*, 15.
- (23) Ivanova, A. E.; Burgart, Ya. Y.; Saloutin, V. I. *Chem. Heterocycl. Compd.* **2013**, *49*, 1128.
- (24) Martin, N. H.; Allen, N. W. III.; Brown, J. D.; Kmiec, D. M. Jr.; Vo, L. *J. Mol. Graph. Model.* **2003**, *22*, 127.
- (25) Marek, R. L. A. *Curr. Org. Chem.* **2002**, *6*, 35.
- (26) Heller, S. T.; Natarajan, S. R. *Org. Lett.* **2006**, *8*, 2675.
- (27) Irwin, J. J.; Sterling, T.; Mysinger, M. M.; Bolstad, E. S.; Coleman, R. G. *J. Chem. Inf. Model.* **2012**, *52*, 1757.
- (28) Lipinski, C. A. *J. Pharmacol. Toxicol. Meth.* **2000**, *44*, 235.
- (29) Bedia, C.; Casas, J.; Garcia, V.; Levade, T.; Fabrias, G. *ChemBioChem* **2007**, *8*, 642.
- (30) **25a**: h-AC IC₅₀ = 0.270±0.185 μM; **26a**: h-AC IC₅₀ = 0.380±0.181 μM.
- (31) Abagyan, R.; Raush, E.; Totrov, M. *ICM Manual 3.7*; Molsoft LCC: San Diego, **2013**, 2103.
- (32) Halgren, T. A. *J. Comput. Chem.* **1996**, *17*, 490.
- (33) (a) Abagyan, R.; Totrov, M. *J. Mol. Biol.* **1994**, *235*, 983. (b) Totrov, M. *Protein-ligand docking as an energy optimization problem*, In *Drug-Receptor Thermodynamics: Introduction and Applications*; Raffa, R. B., Ed.; Wiley: New York, **2001**, 603–624.
- (34) Bedia, C.; Casas, J.; Garcia, V.; Levade, T.; Fabrias, G. *ChemBioChem* **2007**, *8*, 642.
- (35) Bligh, E. G.; Dyer, W. J. *Can. J. Biochem. Physiol.* **1959**, *37*, 911.
- (36) Basit, A.; Piomelli, D.; Armirotti, A. *Anal. Bioanal. Chem.* **2015**, *407*, 5189.